Effect of Pressure on the Oxidative Coupling of Methane in the Absence of Catalyst

Q. Chen, P. M. Couwenberg, and G. B. Marin
Laboratorium voor Chemische Technologie, Eindhoven University of Technology, 5600 MB Eindhoven, The Netherlands

The oxidative coupling of methane was carried out in the absence of catalyst in a continuous flow setup at total pressures up to 1,000 kPa, temperatures from 950 to 1,230 K, and inlet molar ratios of CH_4/O_2 down to 2.5. At constant temperature and residence time, the conversions of methane and oxygen increase drastically with increasing pressure. At oxygen conversions higher than 80%, product selectivities are comparable at different pressures. The space-time yield of the C_2 products reaches a level comparable to that required for industrial operations from 400 kPa on. A radical-reaction network consisting of 38 elementary reactions allows to describe the experimental data. To describe adequately the effect of total pressure, the pressure fall-off behavior of the rate coefficients for the unimolecular reactions in the network has to be taken into account explicitly.

General features of the reaction mechanism do not depend on the total pressure. Methyl and hydrogen peroxy radicals are the most abundant radicals. The total pressure increase results in a drastic increase of the concentrations of the chain carriers, particularly the hydrogen peroxy radical. Higher pressures favor the oxidative route from ethane to ethylene compared to the pyrolytic route. Increasing the total pressure leads to an increase of the primary and a decrease of the consecutive CO formation relative to the coupling. The balance between these nonselective routes determines the effect of the total pressure on the integral selectivity to C_2 products at different conversions. The major contribution to the integral CO selectivity comes from the oxidation of methyl radicals.

Introduction

The noncatalytic partial oxidation of methane, the major constituent in natural gas, to fuels or chemicals has attracted a lot of research efforts. Three alternative routes exist. The partial combustion of methane to synthesis gas, that is, carbon monoxide and hydrogen is the most established (Brophy, 1985; Howard, 1989); the partial oxidation of methane to methanol (Yarlagadda et al., 1988; Foulds et al., 1992; Walsh et al., 1992); and finally, methane can be oxidatively coupled to C_2 hydrocarbons (Lane and Wolf, 1988; Chen et al., 1991; Choudhary et al., 1991).

The oxidative coupling of methane is usually carried out in the presence of catalysts (Lunsford, 1990; Baerns and Ross, 1990). Reactions in the gas phase, however, are believed to play an essential role in the formation of coupling products. A heterogeneous-homogeneous mechanism which emphasizes the importance of the gas-phase reactions has generally been accepted.

The oxidative coupling of methane occurs in the absence of catalyst at temperatures around 1,073 K. However, a ten to hundred times higher space time is needed to reach the same conversion as in the presence of catalyst. Raising the reaction pressure results in an increase of the space-time yields in the absence of catalyst to a level comparable with that obtained in the presence of catalyst (Chen et al., 1992). Furthermore, increasing the pressure is beneficial for the downstream separation train. Therefore, several studies have explored the effect of pressure on the oxidative coupling of methane in the absence of catalyst (Asami et al., 1988; Onsager et al., 1989; Chen and Marin, 1991). Some data on the oxidative coupling

Correspondence concerning this article should be addressed to G. B. Marin.

of methane in the absence of catalyst at elevated pressure have also been reported as blank experiments, that is, when the catalytic coupling was investigated (Ekstrom et al., 1990; Hutchings et al., 1988; and Tulenin et al., 1992a and 1992b).

The modeling of the oxidative coupling of methane in the absence of catalyst has been reported in several articles (Geerts et al., 1990; Zanthoff and Baerns, 1990; Chen et al., 1991; Mackie, 1991; Tjatjopoulos and Vasalos, 1992). Such modeling is based on a radical mechanism of the reaction. Chen et al. (1991) adequately described the experimentally observed conversion-vs.-space-time behavior at atmospheric pressure and low methane conversions. The important chains to various products were identified based upon a contribution analysis. Ethane is mainly formed from the recombination of methyl radicals arising from degenerate branched chains involving OH and HO_2 as main chain carriers. The decomposition of hydrogen peroxide, H_2O_2, is the predominant chain-branching step. Ethylene originates from ethane mainly via a pyrolytic chain, while the oxidative dehydrogenation contributes to a much lower extent. Carbon monoxide originates from the oxidation of methyl radicals, whereas the contribution of the consecutive oxidation of C_2 intermediates or products is not significant at low conversions. Attempts to extend this model to the elevated pressure region were reported (Chen and Marin, 1991). Only limited success was achieved, however, and an adequate description of experiments was only obtained at pressures up to 400 kPa. Zanthoff and Baerns (1990) also reported the simulation of oxidative coupling of methane experiments in the absence of catalyst. The observed selectivities were adequately simulated as a function of the oxygen conversion at a pressure of 400 kPa. The experiments of Onsager et al. (1989) covered a temperature range from 773 to 1,073 K and a pressure range from 300 to 4,000 kPa. Mackie (1991) simulated some of these experiments at low temperatures and high pressures, that is, conditions at which the production of methanol and methanal is favored. Satisfactory agreement between the simulated conversions and selectivities was obtained.

McCarty (1992) constructed a heterogeneous-homogeneous model, which considered a few elementary steps occurring on the catalyst surface in addition to the gas-phase reactions. The oxidative coupling of methane was simulated with this model at pressures up to 10 MPa. No validation by comparison with experiments was made, however. Labinger and Ott (1987) reported a model for the reaction over a mixed Mn-Mg oxide in

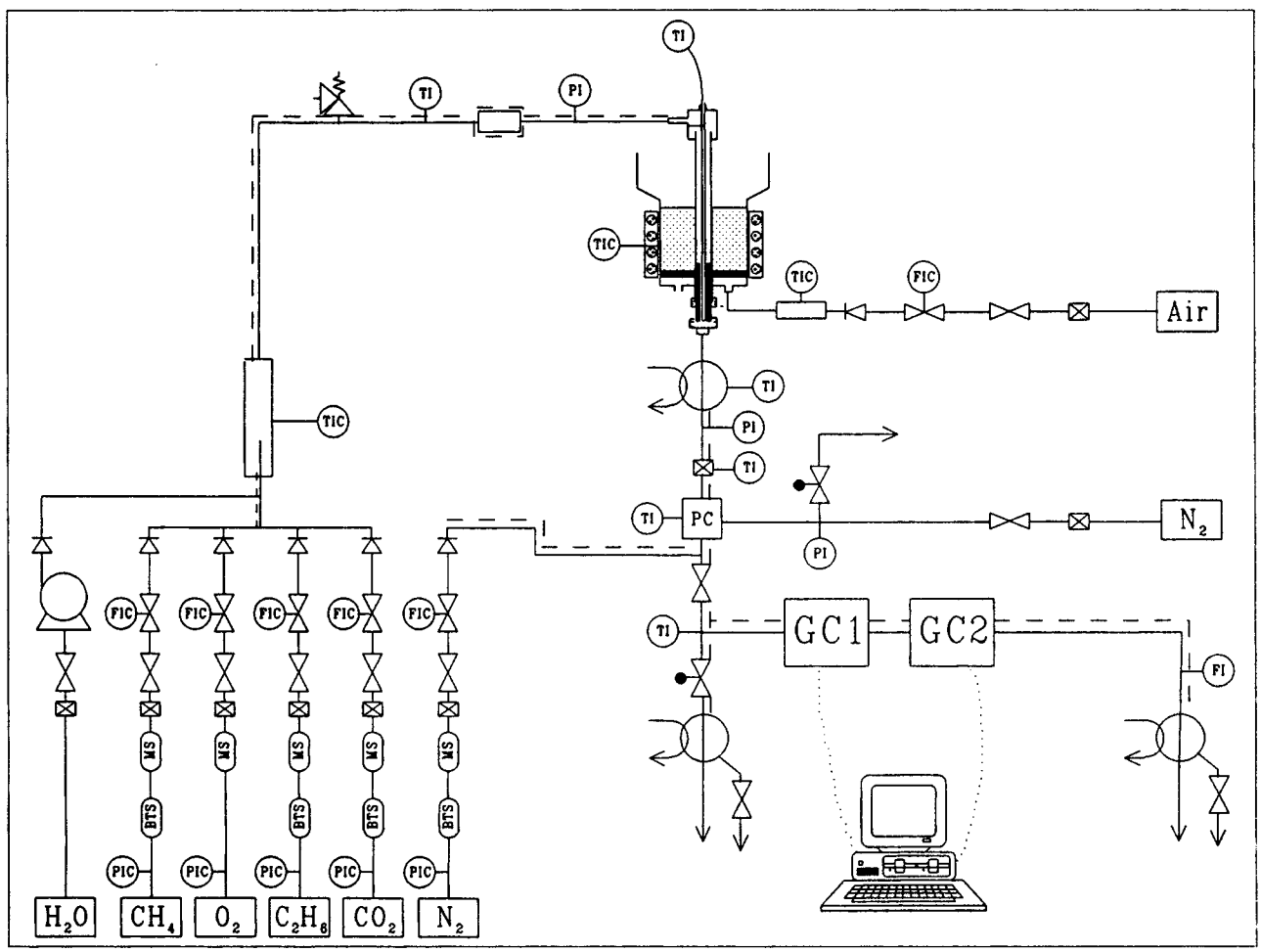

Figure 1. Experimental setup.

Symbols: MS, columns packed with the molsieve particles for water removal; *C*, controller; *F*, flow; *I*, indicator; *P*, pressure; *T*, temperature. TIC represents temperature indication and control, and so on.

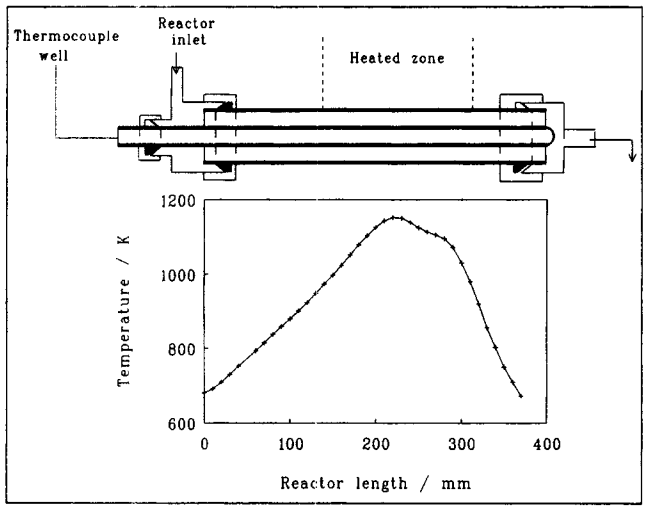

Figure 2. Tubular reactor and a typical axial temperature profile.

the redox-cycle operation mode. Since no gas-phase oxygen was involved, the branched-chain feature of gas-phase reactions could not be disclosed.

The present study concerns the modeling of the oxidative coupling of methane in the absence of catalyst up to a total pressure of 1 MPa and a methane conversion of 32%. On the basis of previous studies (Chen et al., 1991), a model is developed to cover the complete range of conditions, including the higher pressure and higher conversion regions. A reaction path analysis is carried out to identify the important chains in these regions. The shifts in the importance of the different reaction paths are analyzed and explained.

Experimental

Equipment

All experiments were carried out in a continuous flow setup with an empty tubular reactor. The experimental setup is shown in Figure 1. Four gas streams could be set by thermal mass-flow controllers over a wide range making it possible to feed mixtures that are comparable to natural gas or to reactor feeds in a process with recycle. The reactants were premixed before entering the reactor. The maximum capacity of the flowmeters was chosen such that the flow rates used during experiments were lying in the middle or top of the scale. The reactants were not diluted, that is, no inert gas was added.

The reactor was heated with a fluidized sand bath in order to obtain a uniform outside wall temperature. The sand bath was heated with an electrical oven with a temperature controlled on the basis of a thermocouple located between the oven and the sand bath. The reactor and the well were made of nonporous sintered α-alumina. The inner diameter of the alumina tube was 8 mm, the outer diameter of the thermowell was 4 mm, and the length of the tube was 0.65 m. The axial temperature profile in the reactor was measured during every experiment through a thermocouple well located along the axis of the reactor. Figure 2 shows a typical axial temperature profile. The maximum temperature in the profile will be referred to as the reaction temperature, T_{max}. Only that part of the tube where the temperature was higher than 673 K was considered as reactor. The reactor pressure was controlled by a back pressure regulator (Grove Mity Mite). All the devices and the lines in the setup were heated up to 430 K in order to prevent water condensation. After leaving the reactor the product gases were cooled to 450 K with an oil quench. Nitrogen was used as an internal standard and added to the reactor effluent immediately downstream of the pressure regulator.

A fraction of the reactor effluent was directed to the on-line analysis section. The products were analyzed by two gas chromatographs (Hewlett Packard 5890 series II). One of the gas chromatographs is equipped with a Molsieve-5A column (530 μm, 25 m) with helium as carrier gas for the analysis of N_2, O_2, CH_4 and CO, and a Molsieve-5A column with argon as carrier gas for the analysis of H_2 and CH_4. Both columns are connected to a thermal conductivity detector. The other gas chromatograph is equipped with a poraplot-Q (530 μm, 30 m) and a Carbowax column in series, which are connected to a thermal conductivity detector, for the analysis of CH_4, CO_2 and H_2O, and to a flame ionization detector in series for the analysis of CH_4, CH_2O, CH_3OH, C_2H_2, C_2H_4, C_2H_6, C_3H_6 and C_3H_8. Methane appeared in all four cases and, hence, was used as a reference. A complete analysis of the effluent requires 20 min. ChemStation was used for data acquisition. The major products in the present experiments were ethane, ethylene, carbon monoxide, carbon dioxide, hydrogen and water with a minor amount of C_3 products and methanal.

The gases used as reactants were purchased from Hoekloos with purities of 99.999% for nitrogen, 99.995% for oxygen and methane, and 99.5% for ethane.

The reactor and the thermocouple well were pretreated to remove any possible contaminations. The pretreatment procedure consisted of three steps: (a) dipping the tubes in a 60% HNO_3 solution for half an hour; (b) washing the tubes with distilled water; and (c) baking the tubes in an oven at 1,123 K in air for two hours.

Conversions, selectivities and space time

The use of an internal standard allows to measure the flow rates of each product at the reactor outlet and to verify the total mass balance and the C, H and O balances. The molar flow rate of methane at the reactor outlet was calculated from the flow rate of the internal standard, according to:

$$F_{CH_4} = F_{N_2,0} \frac{A_{CH_4}}{A_{N_2}} \frac{d_{N_2}}{d_{CH_4}} \tag{1}$$

The molar flow rate of any species at the reactor outlet was calculated using methane as a reference:

$$F_i = F_{CH_4} \frac{A_i}{A_{CH_4}} \frac{d_{CH_4}}{d_i} \tag{2}$$

The mass balances of carbon, hydrogen and oxygen elements can be easily verified by comparing the inlet flow rates measured with the mass flowmeters and the outlet flow rates obtained from Eq. 1 and Eq. 2 according to:

$$\text{Balance of element } j = \frac{\Sigma\, n_{j,i} F_i}{\Sigma\, n_{j,i} F_{i,0}} \tag{3}$$

where $n_{j,i}$, is the number of atoms of element j (carbon, oxygen or hydrogen) in species i. The balances were closed within 5% for all the experiments.

The conversions and integral selectivities are defined as:

$$X_i = 1 - \frac{F_i}{F_{i,0}}, \quad i = CH_4,\ O_2 \tag{4}$$

$$S_{i,CH_4} = \frac{n_{C,i}(F_i - F_{i,0})}{(F_{CH_4,0} - F_{CH_4})} \tag{5}$$

and calculated according to the so-called normalization method, that is, assuming 100% C- and O-balances. In the present work, the integral selectivity is referred to unless otherwise specified. The calculation of conversions and selectivities does not require the inlet flow rates nor any of the outlet flow rates, but only peak surface areas, if only methane and oxygen are used as reactants:

$$X_i = 1 - \frac{n_{j,i}A_i/d_i}{n_{j,i}A_i/d_i + \Sigma\,(n_{j,k}A_k/d_k)}, \quad i = CH_4,\ O_2 \text{ and } j = C,\ O \tag{6}$$

The integral selectivity of product i with respect to methane is calculated according to:

$$S_{i,CH_4} = \frac{n_{C,i}A_i/d_i}{\Sigma(n_{C,k}A_k/d_k)}, \quad i = \text{any product} \tag{7}$$

In Eq. 6 and Eq. 7, the summations with index k are with respect to all the carbon containing components in the reactor effluent, except methane for the calculation of the methane conversion and product selectivities, and with respect to all the oxygen containing components, except dioxygen, for the calculation of the oxygen conversion.

The product of the conversions of methane and the selectivity towards ethane and ethylene is referred to as the C_2 product yield.

In the present work, both space time and residence time were used. The space time is used as an independent variable during the integration of the continuity equations (Chen et al., 1991) and is defined as follows:

$$\text{Space time} = \frac{V}{F_{CH_4,0}} \tag{8}$$

The residence time is defined according to Plehiers and Froment (1987):

$$\tau = \int_0^V \frac{p_t dV}{FRT} \cong \frac{\Omega p_t}{F_0 R} \int_0^l \frac{dz}{T} \tag{9}$$

where z is the length coordinate in the reactor, m; l, total length of the reactor, m; p_t, total pressure, Pa; F_0, total molar inlet flow rate, mol·s^{-1}; V, volume of the reactor, m^3; and Ω, cross-sectional surface area of the reactor, m^2 and calculated from:

$$\tau = \frac{\Omega p_t}{F_0 R} \Sigma \frac{\Delta z}{T} \tag{10}$$

Table 1. Range of Experimental Conditions

Total pressure/100 kPa	1-10
Maximum axial temperature/K	950-1,230
Inlet molar ratio CH_4/O_2	2.5-10.0
Space time/m^3·s·mol^{-1}	0.0042-0.91
Residence time/s	0.32-9.0
CH_4 conversion/%	1-32
O_2 conversion/%	6-100

Clearly, for a correct calculation of the residence time, the axial temperature profile is a necessity.

Conditions

The experiments covered a wide range of conditions which is summarized in Table 1. A total of 50 experiments were performed.

Effects of Process Conditions

Total pressure

Conversions. Figure 3 shows the conversions of methane and oxygen as a function of the total pressure at two inlet methane-to-oxygen ratios. The residence time was kept constant at 0.5s in order to have a common basis for comparison. At atmospheric pressure, no reaction was observed under similar conditions. The conversions increase sharply with increasing total pressure. This effect has been reported in the literature (Asami et al., 1988; Ekstrom et al., 1990). The effect of pres-

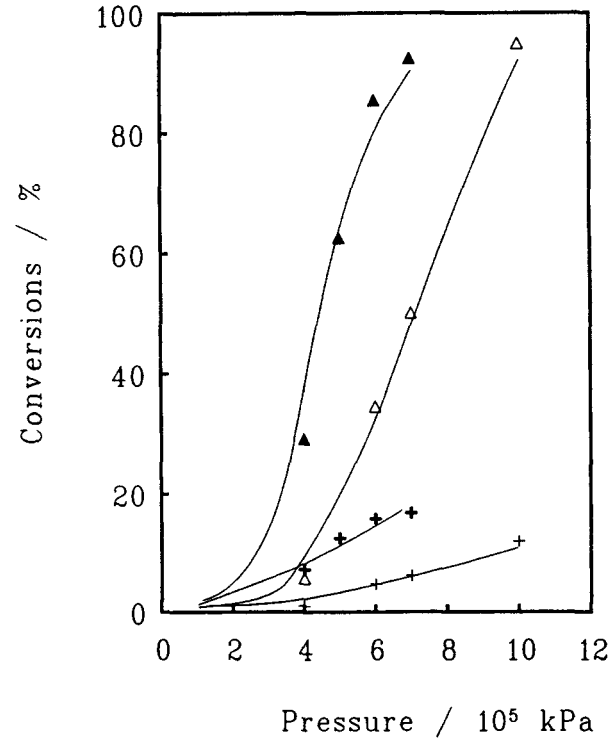

Figure 3. Effect of total pressure on the conversions of methane and oxygen.

Full lines: calculated with the model shown in Table 2; points: experimental; +, CH_4, Δ, O_2 at δ = 10.0, +, CH_4, ▲, O_2 at δ = 5.0. T_{max} = 1,090 K, τ = 0.5 s.

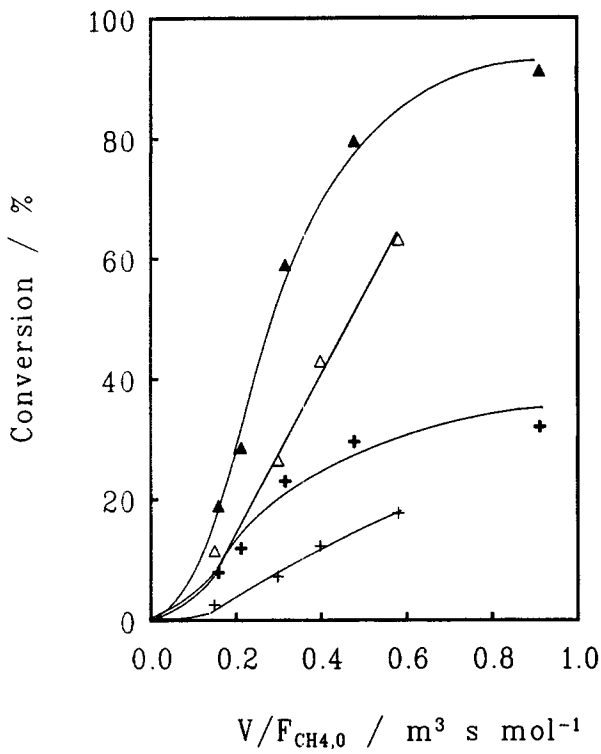

Figure 4. Conversions of methane and oxygen vs. space time at 100 kPa.

Full lines: calculated with the model shown in Table 2; points: experimental; +, CH_4, ▵, O_2 at δ = 4.0, +, CH_4, ▲, O_2 at δ = 2.5 T_{max} = 1,100 K.

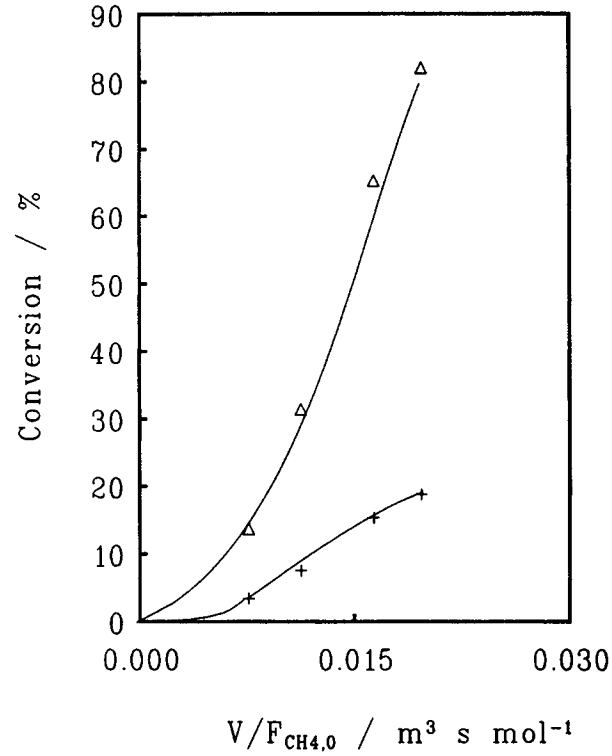

Figure 5. Conversions of methane and oxygen vs. space time at 400 kPa.

Full lines: calculated with the model shown in Table 2; points: experimental; +, CH_4, ▵, O_2; at δ = 4.0, T_{max} = 1,078 K.

sure on conversions can also be seen by comparing Figure 4 with Figure 5. The space time required to reach a certain conversion at 100 kPa is one order of magnitude larger than at 400 kPa, in spite of the higher temperature used during the experiments at 100 kPa. Figure 6 shows the increase of the methane conversion rates with the total pressure at a residence time of 0.5s. The former was calculated from the methane conversion divided by the space time. Clearly, the pressure dependence of the methane conversion rate is stronger than quadratic.

Space-Time Yield of C_2 Products. Also shown in Figure 6 are the space-time yields of the C_2^+ products, defined as moles of C_2^+ products produced per unit reactor volume per second. This can be considered as an average C_2^+ production rate in a reactor which is operated in an integral way. Weisz (1982) noted that the space-time yields in most processes in the petroleum refining and petrochemical industry fall in a window of approximately 1 to 10 mol·m$^{-3}_{reactor}$·s^{-1}. The C_2H_4 space-time yield in an ethane steam cracking plant, for example, amounts to 12 mol·m^{-3}·s^{-1} based on the radiation section. The lower limit of the window corresponds to uneconomically high investment costs, while the upper limit corresponds to limitations by the transport of mass and/or heat. It is clear from Figure 6 that the space-time yields of C_2 products are within the window for industrial applications in the pressure range of 400 kPa up to 1,000 kPa. The space-time yield of C_2^+ at 100 kPa, however, is too low. Raising the pressure from 100 to 400 kPa increases the space-time yield by more than one order of magnitude. The pressure dependence of the space-time yield increases from quadratic to cubic when increasing the inlet methane-to-oxygen ratio from 5 to 10.

Selectivities. The selectivity to the C_2 products generally decreases with increasing conversion. The effect of process conditions on the selectivity observed experimentally can thus be disguised by a simultaneous conversion change. Therefore, the experimental determination of the effect of total pressure on the selectivity requires the comparison of complete sets of selectivity vs. conversion data at different total pressures. Figure 7 shows the selectivity to the major carbon-containing products as a function of the oxygen conversion at 100 kPa and 400 kPa. The trends of the selectivity change as a function of conversion are similar at both pressures. The selectivity to both CO and CO_2 increases and that to CO increases more strongly. The ethylene selectivity increases with the conversion while the ethane selectivity decreases. This indicates that ethylene originates from ethane. At low conversions, the selectivity to ethylene decreases by 4 to 8% with a pressure increase from 100 to 400 kPa. This decrease is accompanied with an increase of the selectivity to CO by up to 8%. With the increase of the conversion, this decrease becomes smaller and disappears at oxygen conversions around 80%.

Also, an appreciable selectivity to methanal, CH_2O, was observed in the experiments at elevated pressures, while no methanal was detected at atmospheric pressure. The maximum selectivity to methanal amounted to 13% at a methane conversion of 4.4% and an oxygen conversion of 22% at 400 kPa, 950 K and an inlet methane-to-oxygen molar ratio of 4.0. The production of methanal in the methane oxidation is not unexpected. It is well known that methanal plays the role of

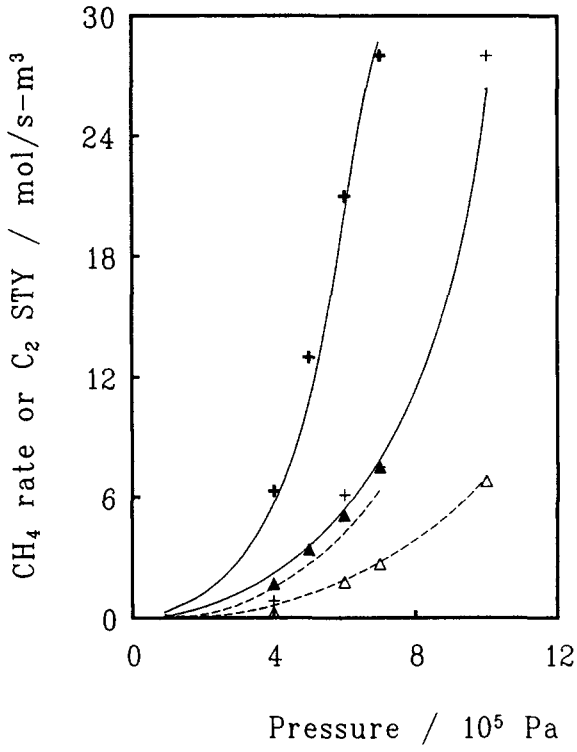

Figure 6. Rate of conversion of methane and the space time yield of C_2 as a function of total pressure.

Lines: calculated with the model shown in Table 2; solid lines: rate of conversion of methane, dashed lines: space time yield of C_2. Points: experimental; +, and +, rate of conversion of methane at δ = 10.0 and 5.0; $\triangle$ and $\blacktriangle$, C_2 space time yields at δ = 10.0 and 5.0. T_{max} = 1,090 K, τ = 0.5 s.

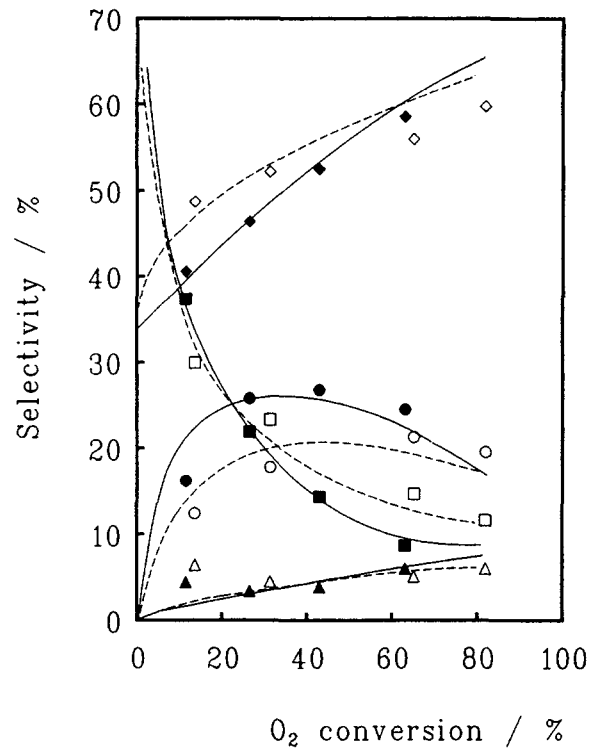

Figure 7. Selectivities for the main reaction products vs. oxygen conversion.

Lines: calculated with the model shown in Table 2; points: experimental; ○, ●, C_2H_4, □, ■, C_2H_6, ◇, ◆, CO and $\triangle$, $\blacktriangle$, CO_2. Solid lines and filled points: p_t = 100 kPa and T_{max} = 1,100 K; dashed lines and empty points: p_t = 400 kPa and T_{max} = 1,078 K. δ = 4.0.

intermediate for the formation of carbon monoxide (Semenov, 1958; Warnatz, 1983; Chen et al., 1991). Hargreaves et al. (1991) reported a maximum methanal selectivity of higher than 60% at a temperature of 1,025 K and atmospheric pressure, when the oxygen conversion was below 10%. Beyond this conversion, the methanal selectivity dropped to zero. Walsh et al. (1992) reported that the methanal production is favored over the C_2 production at low temperatures and high pressure and the methanal production decreases with the increase of conversion and temperature. This was also observed in the present experiments. For example, the methanal selectivity decreases to 0.5% at an oxygen conversion of 82% at 400 kPa, 1,073 K and an inlet methane-to-oxygen molar ratio of 4.0.

Small amounts of C_3 hydrocarbons were detected in all experiments. They were identified as propene and propane. The maximum selectivity amounted to 4.3% for propene and 1.2% for propane at 1 MPa, 1,100 K and an inlet methane-to-oxygen molar ratio of 10.0. The C_3 products originate from the consecutive reactions of C_2 products, for example, through the addition of C_1 species. Oxygen-containing species are usually not involved. This is evidenced by the fact that higher inlet methane-to-oxygen ratios resulted in higher C_3 selectivities. In general, the selectivity to C_3 products was higher at high pressure than at atmospheric pressure for a given conversion.

The dihydrogen selectivity increases with conversions at both atmospheric and elevated pressure. Dihydrogen can be formed from two sources via two independent routes, both of consecutive nature. One route is the decomposition of the hydrogen-containing products, for example, ethane and methanal, and the other is the water-gas shift reaction. At high conversions more ethane and CO, and thus dihydrogen, are produced. Ekstrom et al. (1990) also reported that the pressure increase resulted in a marked increase in hydrogen yields. However, since the conversion in their experiments was not kept constant at different pressures, the increase in hydrogen yield is again rather an effect of conversion increase than an effect of pressure increase. Also, the ratio of hydrogen to water increased with increasing conversions. This can be expected from the water-gas shift reaction. This is in contrast to the results of Asami et al. (1988) who observed a constant hydrogen to water ratio between 4.2 and 4.3.

Inlet methane-to-oxygen ratio

Figure 4 clearly shows that at a given space time, the conversions at an inlet methane-to-oxygen ratio of 2.5 are much higher than at a ratio of 4.0. The effect of an increasing inlet methane-to-oxygen ratio on the product selectivities is not very pronounced at a given methane conversion. At the inlet methane-to-oxygen molar ratio of 2.5, the selectivity to ethylene decreases by up to 4% compared to that at the ratio 4, while the selectivity to CO increases accordingly. At lower inlet methane-to-oxygen ratios the space-time yield of C_2^+ products increases as well, as is shown in Figure 6. Both the methane conversion rate and the space-time yield of C_2^+ products are one order of magnitude higher at an inlet methane-to-oxygen

molar ratio of 5.0 than at an inlet methane-to-oxygen molar ratio of 10.0.

Temperature

Experiments have been carried out at a total pressure of 400 kPa and constant residence time while the temperature was varied from 950 to 1,230 K. The temperature refers to the maximum temperature in the axial temperature profile. The residence time was chosen such that over the complete temperature range the maximum oxygen conversion remains under 95% in order to avoid stoichiometric limitations by oxygen. The temperature dependence at a total pressure of 400 kPa is quite similar to that at 100 kPa. As is expected, the conversions increase when the temperature is increased. At 400 kPa and an inlet methane-to-oxygen ratio of 4.0, the space-time yield of C_2 products increases from 0.8 $mol \cdot m^{-3} \cdot s^{-1}$ at 1,000 K to 1.6 $mol \cdot m^{-3} \cdot s^{-1}$ at 1,052 K due to the increase of the methane conversion. This is small when compared to the effect of total pressure on the space-time yield.

It is clear from the above discussion that the experimental determinations of the effect of a single process condition on the product distribution is difficult because of the strong negative correlation between the C_2 selectivity and the conversions. The availability of a reliable kinetic model would remedy this difficulty and would allow a straightforward calculation of the effects of the process conditions. Furthermore, kinetic modeling leads to a better understanding of the reaction paths through which the coupling occurs.

Modeling

The procedures for the model development have been described in detail previously (Chen et al., 1991). A brief summary is given below. A reaction network composed of elementary radical reactions was constructed. It was shown that at atmospheric pressure heterogeneous terminations of radicals at the reactor wall could be neglected when compared with homogeneous terminations, and, hence, *a fortiori* at higher pressures. The Arrhenius parameters for each step were taken from the literature on combustion chemistry (Tsang and Hampson, 1986; Tsang, 1988; Warnatz, 1983, 1984). Only the Arrhenius parameters for the forward steps were needed, while those for the reverse steps were calculated from thermodynamics. The reactor model consisted of a set of continuity equations describing the concentration of every molecule or radical in the axial direction of the plug-flow reactor. The plug-flow assumption was justified on the basis of a criterion derived by Cleland and Wilhelm (1956) for viscous-flow tubular reactors. This resulted in a set of stiff first-order ordinary differential equations. The method developed by Dente et al. (1979), applying the pseudo-steady-state approximation for the reactive radicals, was used for the integration of the equations. The measured axial temperature profile was taken into account explicitly during the integration of the continuity equations. A contribution analysis and a sensitivity analysis were performed and allowed to identify the important reactions. By definition, the contribution factor of a step with respect to the disappearance of a species is the ratio of the consumption rate of the species in this step to the total consumption rate of the species.

Network construction

The construction of the radical reaction network started from the 66-reaction-model of the previous study (Chen et al., 1991). Some less important reactions were removed from the network and the reactions involving C_3 hydrocarbons were added since their yields were too high to be neglected. Although a large number of reactions which involve C_3 components were considered initially, the final model consists of only four such reactions. After the parameter estimation was completed, the network was further reduced by removing reactions found to be unimportant by a sensitivity analysis. The final network consists of 38 reactions among 13 molecules and 10 radicals, as is shown in Table 2. The molecules are: dihydrogen, water, hydrogen peroxide, dioxygen, methane, methanal, carbon monoxide, carbon dioxide, ethyne, ethylene, ethane, propene and propane. The radicals are: hydrogen and oxygen atoms, hydroxy, hydrogen peroxy, formyl, methoxy radicals and methyl, vinyl, ethyl and propyl radicals. In the right half of Table 2, the first two columns list the preexponential factor and activation energy for the forward step of each reaction. The third column gives dimensionless affinities. The affinity for a reaction is defined as the Gibbs energy difference of the reaction with a minus sign. The last column shows rates of the forward steps. The rate of a reaction and of the backward step can be easily deduced from the affinity and the rate of the forward step according to:

$$\begin{aligned} \overleftarrow{r} &= \vec{r} \exp\left(-\frac{A}{RT}\right) \\ r &= \vec{r} - \overleftarrow{r} = \vec{r}\left[1 - \exp\left(-\frac{A}{RT}\right)\right] \end{aligned} \tag{11}$$

The affinities and the forward rates reported in Table 2 were calculated at the maximum temperature in the reactor. The corresponding conversions of methane and oxygen amounted to 12% and 41%.

Parameter estimation

The majority of the Arrhenius parameters was taken from the previous study (Chen et al., 1991). For reactions which were not considered in that study, the parameters were selected from databases originated from combustion chemistry (Tsang and Hampson, 1986; Tsang, 1988; Warnatz, 1983, 1984). The work of Geerts et al. (1990) and Zanthoff and Baerns (1990) served as supplementary sources.

The important reactions were identified through a contribution analysis and a sensitivity analysis. The parameters of these steps were adjusted by means of regression of experimental data, and the adjusting can be justified as follows. It is well recognized that values of the Arrhenius parameters reported by different workers deviate from each other by orders of magnitude. Another widely-accepted fact is that the Arrhenius parameters are lying within a certain range rather than being uniquely determined. The uncertainty factor of a parameter can be as large as 10 (Tsang and Hampson, 1986). Secondly, the values taken from the literature were normally applied to combustion and could not describe experimental observations in this work nor any of those reported in the literature on the oxidative coupling of methane without ad-

Table 2. Model for the Oxidative Coupling of Methane in the Absence of Catalyst Covering the Range of Conditions Given in Table 1

Step No.	Reaction	A	E_a	A/RT^*	r^*
(1)	$CH_4 + O_2 \rightleftarrows CH_3 + HO_2$	$0.983 \times 10^{+07}$	193.86	−1.4	$0.694 \times 10^{+00}$
(2)	$CH_4 + H \rightleftarrows CH_3 + H_2$	$0.234 \times 10^{+09}$	51.17	0.7	$0.314 \times 10^{+02}$
(3)	$CH_4 + O \rightleftarrows CH_3 + OH$	$0.127 \times 10^{+10}$	33.83	8.4	$0.732 \times 10^{+00}$
(4)	$CH_4 + OH \rightleftarrows CH_3 + H_2O$	$0.743 \times 10^{+09}$	41.43	3.2	$0.570 \times 10^{+02}$
(5)	$CH_4 + HO_2 \rightleftarrows CH_3 + H_2O_2$	$0.401 \times 10^{+08}$	99.61	2.4	$0.141 \times 10^{+02}$
(6)	$CH_3 + O_2 \rightleftarrows CH_3O + O$	$0.308 \times 10^{+09}$	141.00	20.9	$0.111 \times 10^{+00}$
(7)	$CH_3 + O_2 \rightleftarrows CH_2O + OH$	$0.459 \times 10^{+08}$	103.66	38.4	$0.107 \times 10^{+01}$
(8)	$CH_3 + HO_2 \rightleftarrows CH_3O + OH$	$0.900 \times 10^{+08}$	0.00	30.7	$0.300 \times 10^{+02}$
(9)	$CH_3 + CH_3 + M \rightleftarrows C_2H_6 + M$	$0.650 \times 10^{+08}$	0.00	4.8	$0.124 \times 10^{+02}$
(10)	$CH_3O + M \rightleftarrows CH_2O + H + M$	$0.258 \times 10^{+15}$	115.00	3.3	$0.314 \times 10^{+02}$
(11)	$CH_2O + OH \rightleftarrows CHO + H_2O$	$0.580 \times 10^{+09}$	5.00	9.1	$0.132 \times 10^{+01}$
(12)	$CH_2O + HO_2 \rightleftarrows CHO + H_2O_2$	$0.417 \times 10^{+07}$	40.12	8.3	$0.572 \times 10^{+00}$
(13)	$CH_2O + CH_3 \rightleftarrows CHO + CH_4$	$0.700 \times 10^{+08}$	25.03	5.9	$0.308 \times 10^{+02}$
(14)	$CHO + M \rightleftarrows CO + H + M$	$0.280 \times 10^{+10}$	64.36	4.8	$0.332 \times 10^{+02}$
(15)	$CHO + O_2 \rightleftarrows CO + HO_2$	$0.171 \times 10^{+06}$	0.00	9.1	$0.332 \times 10^{+00}$
(16)	$CO + HO_2 \rightleftarrows CO_2 + OH$	$0.308 \times 10^{+09}$	107.34	36.3	$0.260 \times 10^{+01}$
(17)	$C_2H_6 + H \rightleftarrows C_2H_5 + H_2$	$0.910 \times 10^{+09}$	51.70	2.3	$0.158 \times 10^{+01}$
(18)	$C_2H_6 + OH \rightleftarrows C_2H_5 + H_2O$	$0.455 \times 10^{+09}$	17.12	4.8	$0.722 \times 10^{+01}$
(19)	$C_2H_6 + CH_3 \rightleftarrows C_2H_5 + CH_4$	$0.225 \times 10^{+08}$	64.57	1.6	$0.322 \times 10^{+01}$
(20)	$C_2H_5 + HO_2 \rightleftarrows CH_3 + CH_2O + OH$	$0.240 \times 10^{+08}$	0.00	33.4	$0.629 \times 10^{+00}$
(21)	$C_2H_5 + M \rightleftarrows C_2H_4 + H + M$	$0.596 \times 10^{+14}$	167.66	0.6	$0.134 \times 10^{+02}$
(22)	$C_2H_5 + O_2 \rightleftarrows C_2H_4 + HO_2$	$0.635 \times 10^{+07}$	53.20	4.9	$0.326 \times 10^{+01}$
(23)	$C_2H_4 + O_2 \rightleftarrows C_2H_3 + HO_2$	$0.281 \times 10^{+07}$	144.55	2.1	$0.569 \times 10^{+00}$
(24)	$C_2H_4 + H \rightleftarrows C_2H_3 + H_2$	$0.150 \times 10^{+09}$	42.70	4.2	$0.606 \times 10^{+00}$
(25)	$C_2H_4 + OH \rightleftarrows C_2H_3 + H_2O$	$0.612 \times 10^{+08}$	24.70	6.7	$0.354 \times 10^{+00}$
(26)	$C_2H_4 + CH_3 \rightleftarrows C_2H_3 + CH_4$	$0.199 \times 10^{+06}$	51.46	3.5	$0.104 \times 10^{+00}$
(27)	$C_2H_4 + OH \rightleftarrows CH_3 + CH_2O$	$0.688 \times 10^{+07}$	0.00	3.6	$0.628 \times 10^{+00}$
(28)	$C_2H_3 + M \rightleftarrows C_2H_2 + H + M$	$0.121 \times 10^{+16}$	176.44	−2.1	$0.121 \times 10^{+00}$
(29)	$C_2H_3 + O_2 \rightleftarrows C_2H_2 + HO_2$	$0.500 \times 10^{+07}$	0.00	2.2	$0.106 \times 10^{+01}$
(30)	$C_2H_3 + O_2 \rightleftarrows CH_2O + CHO$	$0.500 \times 10^{+07}$	0.00	44.4	$0.106 \times 10^{+01}$
(31)	$C_2H_5 + CH_3 \rightleftarrows C_3H_8$	$0.800 \times 10^{+07}$	0.00	5.2	$0.124 \times 10^{+00}$
(32)	$C_3H_8 + H \rightleftarrows C_3H_7 + H_2$	$0.900 \times 10^{+09}$	32.00	2.0	0.844×10^{-01}
(33)	$C_2H_4 + CH_3 \rightleftarrows C_3H_7$	$0.300 \times 10^{+06}$	29.00	0.2	$0.194 \times 10^{+01}$
(34)	$C_3H_7 + \rightleftarrows C_3H_6 + H$	$0.150 \times 10^{+16}$	156.00	0.1	$0.135 \times 10^{+01}$
(35)	$O_2 + H \rightleftarrows OH + O$	$0.220 \times 10^{+09}$	70.30	19.4	$0.616 \times 10^{+00}$
(36)	$O_2 + H + M \rightleftarrows HO_2 + M$	$0.140 \times 10^{+06}$	0.00	4.3	$0.452 \times 10^{+02}$
(37)	$HO_2 + HO_2 \rightleftarrows O_2 + OH + OH$	$0.200 \times 10^{+07}$	0.00	24.9	$0.112 \times 10^{+01}$
(38)	$H_2O_2 + M \rightleftarrows OH + OH + M$	$0.127 \times 10^{+12}$	199.36	21.2	$0.131 \times 10^{+02}$

* Calculated at the point in the reactor where the temperature is maximum. Conditions are T_{max} = 1,078 K, p_t = 400 kPa, inlet methane-to-oxygen ratio δ = 4.0 and $V/F_{CH4,0}$ = 0.020 $m^3 \cdot s \cdot mol^{-1}$. The corresponding conversions at the point: X_{CH4} = 12%, X_{O2} = 41%. Units: A, s^{-1} or $m^3 \cdot mol^{-1} \cdot s^{-1}$ or $m^6 \cdot mol^{-2} \cdot s^{-1}$; E_a, $kJ \cdot mol^{-1}$; r, $mol \cdot m^{-3} \cdot s^{-1}$.

justments. Next, the parameters have to be within the physical limits following from theories concerning the rates of elementary gas-phase reactions, such as the transition-state theory (Benson, 1976). Finally, the adjustment was limited to those steps shown to be important either from the contribution analysis or from the sensitivity analysis.

During the minimization of the objective function, the following molecules were used as responses: oxygen, methane, carbon monoxide, carbon dioxide, ethyne, ethylene and ethane. The responses were weighed in such a way that their contributions to the objective function were comparable. Twenty experiments were used for the minimization. The parameters of the following steps in Table 2 were adjusted: 1, 2, 4–10, 12–19, 21, 27, 29, 35, and 38. Compared with the values before the adjustment, the estimation of the parameters resulted in rate coefficients which do not differ from their starting values by more than a factor of 1/5 to 5. Exceptions are the rate coefficients for steps 13 and 15 in Table 2 which have been reduced by a factor of 10 with respect to their starting value at 1,000 K and that for step 14 which has been increased by a factor of 10.

Arrhenius Dependency. Two-parameter Arrhenius relations were adopted in this study. A third parameter is often used in combustion modeling (Chen et al., 1991), when such a modeling is intended to cover a temperature range from room temperature to 2,000 K or higher. Within such a broad range, the temperature dependency of a rate coefficient often deviates from linearity in an Arrhenius diagram. The temperature range in the present study, however, is much narrower. Hence, the third parameter was not necessary. For reactions for which three-parameter Arrhenius relations were reported, the two-parameter relations were derived by linear regression of the logarithm of the rate coefficients vs. $1/T$ over the temperature range of interest for the present study from 700 to 1,100 K.

Pressure Fall-Off. The variation of the kinetic parameters of the unimolecular reactions with pressure was taken into account to describe the effect of pressure adequately. In chemical kinetics, it is well-known that the pseudo-first-order rate coefficient for a unimolecular reaction, k_u, as defined in Eq. 12:

$$A + M \rightarrow A_1 + A_2 + M \quad \text{with} \quad r = k_u C_A \tag{12}$$

decreases with total pressure (Gardiner and Troe, 1984). Such a decrease is called "(pressure) fall-off" of the rate coefficient. The curve of k_u against pressure is called the "fall-off curve" of the unimolecular reaction. In Eq. 12, M denotes a collision partner for species A, better known as the "third body" or "bath gas," which consists of all the species in the reaction mixture. With the increase of total pressure, k_u increases in first approximation according to the classic Lindemann equation:

$$k_u = \frac{kC_M}{1 + kC_M} k_\infty \tag{13}$$

In Eq. 13, the third-body concentration C_M is commonly used in spite of the term "pressure" falloff.

The third-body concentration was taken as the weighed sum of concentrations of all the molecular species. The weight factors, w_i, take into account the relative collision efficiencies of the third bodies:

$$C_M = \Sigma w_i C_i \tag{14}$$

In general, the collision efficiency of a species is dependent on temperature and such a dependence is not the same for different reactions. In the present case, the collision efficiency was considered to be roughly equal for different reactions (Warnatz, 1984), while the temperature dependence could be neglected (Tsang and Hampson, 1986). Thus, constant values were used for the collision efficiencies relative to dihydrogen, most of which were equal to unity. Exceptions are H_2O, O_2, CO and CO_2 with values of 6.5, 0.4, 0.75 and 1.5 (Warnatz, 1983).

At sufficiently high pressures, that is, when $kC_M \gg 1$, it follows from Eq. 13 that k_u is independent of the total pressure and approaches k_∞. At low pressures, that is, when $kC_M \ll 1$, k_u becomes proportional to the total pressure, or the total concentration of "third bodies":

$$k_u = kk_\infty C_M = k_0 C_M, \quad \text{with} \quad k_0 = kk_\infty \tag{15}$$

In the latter case, the reaction is of second-order. The pressure at which the ratio k_u/k_∞ equals 1/2 is referred to as $p_{1/2}$ in the literature. The latter gives a good indication of the importance of the fall-off behavior for a particular reaction.

Note that Eq. 12 and the discussion so far relate to a dissociation step. The reverse step, the recombination reaction:

$$A_1 + A_2 + M \rightarrow A + M \quad \text{with} \quad r = kC_{A1}C_{A2} \tag{16}$$

proceeds via a common intermediate, and the rate coefficient is also dependent on the total pressure. The fall-off behavior for both steps is identical and can be treated in the same way (Gardiner and Troe, 1984). Thus, the rate coefficient for recombination is proportional to total pressure in the low pressure limit and approaches a constant value with increasing pressure. Hence, the recombination is of third-order in the low pressure limit.

Table 3. $p_{1/2}$ Values of the Important Unimolecular Reactions at Different Temperatures (Tsang and Hampson, 1986)

Reaction	$p_{1/2}$/100 kPa 900 K	1,100 K	1,300 K
(9) $CH_3\cdot + CH_3\cdot + M \rightarrow C_2H_6 + M$	0.028	0.093	0.18
(21) $C_2H_5\cdot + M \rightarrow C_2H_4 + H\cdot + M$	0.14	0.48	1.53
(28) $C_2H_3\cdot + M \rightarrow C_2H_2 + H\cdot + M$	0.054	0.10	0.16
(10) $CH_3O\cdot + M \rightarrow CH_2O + H\cdot + M$	—	13	—
(14) $CHO\cdot + M \rightarrow CO + H\cdot + M$	—	10	—
(36) $H\cdot + O_2 + M \rightarrow HO_2\cdot + M$	—	10	—
(38) $H_2O_2 + M \rightarrow OH\cdot + OH\cdot + M$	—	11	—

Various unimolecular reaction rate theories have been elaborated since Lindemann's. The Rice-Ramsperger-Kassel-Marcus (RRKM) theory is the most important and the most widely applied (Robinson and Holbrook, 1972). In their compilations of kinetic databases for combustion chemistry, Tsang and Hampson (1986, 1988) provided the fall-off data for the rate coefficients of most of the unimolecular reactions. Arrhenius expressions at one of the limiting pressures for k_∞ or k_0 were given. Ratios of the rate coefficients k_u/k_∞ or k_u/k_0, resulting from the calculation from the RRKM theory were also tabulated at different temperatures and third-body concentrations. For the rate coefficients for the unimolecular reactions in the present model, Table 2 shows the Arrhenius parameters at one of the limiting pressures, either k_∞ or k_0. They were corrected for the pressure fall-off behavior in the way that is described below.

Ten unimolecular reactions have been included in the final model. They could be divided into three groups, corresponding to the high-pressure, the intermediate and the low-pressure region. The first group consisted of the reactions involving C_3 components 31, 33 and 34 in Table 2. The rate coefficients of these reactions were assumed to have reached the corresponding high pressure limits, k_∞, because of their low $p_{1/2}$ values originated from the large molecules involved. In addition, the experimental yields of these species were low. Thus, these reactions were represented in Table 2 without the third body M. The rate coefficients calculated from the data in Table 2 were used directly, as in Eq. 12.

Table 3 lists the $p_{1/2}$ values for the remaining unimolecular reactions at the temperatures of interest. The $p_{1/2}$ values were obtained by interpolating the tabulated data of Tsang and Hampson, if available. Those for reactions 14 and 36 in Table 3 were estimated, because Tsang and Hampson indicated that these reactions were completely in the low-pressure region at the pressures of interest in the present study. This is confirmed by the estimations reported in Table 3, where it is clear that reactions 10 and 38 are also completely in the low-pressure region. All these reactions are in this region at the present conditions because of the small size of the involved species, that is, due to their lack of internal degrees of freedom. For the calculation of the rate of the forward steps according to Eq. 12, the pseudo-first-order rate coefficient k_u was obtained

by multiplying k_0 with the third-body concentration, C_M, as obtained from Eq. 14.

It follows from Table 3 that the group of reactions for which the pressure fall-off should be taken into account fully consists of reactions 9, 21 and 28. For this group of reactions, the tabulated fall-off data of Tsang and Hampson were correlated with temperature and third-body concentration, as calculated by Eq. 14. The unimolecular rate coefficients, k_u, were obtained by multiplying the rate coefficient k_∞ for 9 and 21 or k_0 for 28 derived from Table 2 by either k_u/k_∞ or k_u/k_0 ratio at the corresponding temperature and third-body concentration. The deviation of k_u from k_∞ or k_0 can be significant under the conditions of the present study. For example, at 1,100 K and 100 kPa k_u/k_∞ amounts to 0.85 for the recombination of two methyl radicals, reaction 9, and to 0.59 for the decomposition of ethyl radical to ethylene, reaction 21 in Table 3.

Simulation results

The conversions of methane and oxygen and the selectivities to various products calculated by means of the model shown in Table 2 are drawn as full lines in the figures. Figures 3, 4 and 5 show the conversions as a function of total pressure or space time. The increase of conversions, resulting from increasing the total pressure from 400 to 1,000 kPa was described adequately by the model, as is shown in Figure 3. This figure also shows that the model correctly extrapolates towards pressures lower than 400 kPa. Indeed, at these pressures, the reaction still proceeds at a rate which did not allow reproducible observations at a residence time of 0.5 s. The present model also describes adequately the complete set of data obtained at atmospheric pressure and reported previously (Chen et al., 1991). Figure 4 shows that even at a methane conversion as high as 32%, the calculated conversions agree well with the experiments. The model also describes the conversion as a function of space time adequately over a broad range of oxygen conversions, as can be seen from Figure 5.

The selectivities calculated with the model are compared with the experimental data in Figure 7 and, indirectly, in Figure 6. The increase of the oxygen conversion was brought about by an increase of the space time. As can be seen from Figure 7, the sharp decrease of the ethane selectivity and the increase of the CO selectivity were simulated correctly at atmospheric pressure. The maximum in the ethylene selectivity is also simulated. At 400 kPa, the calculated CO selectivity at high conversions is slightly higher than the observed selectivity, whereas the corresponding ethylene selectivity is slightly lower than observed.

Reaction Path Analysis

The important chains at low conversions and atmospheric pressure have been discussed previously (Chen et al., 1991). The following discussion focuses the reaction paths at higher conversions and elevated pressures. The differential contribution factors were calculated with the model at the position in the reactor where the temperature is maximum. The conditions for the calculation of the contribution factors were: T_{max} = 1,078 K, p_t = 400 kPa, inlet methane-to-oxygen ratio = 4.0 mol·mol^{-1} and $V/F_{CH4,0}$ = 0.020 m^3·s·mol^{-1}. The corresponding conversions of methane and dioxygen amounted to 12% and 41% at the point of calculation and to 19% and 81% at the reactor outlet. For comparison, the contribution factors were also calculated at a total pressure of 100 kPa with an identical temperature profile and inlet methane-to-oxygen ratio and at a space time leading to the same oxygen conversion at the point of calculation. The corresponding methane conversion amounted to 13%, and the conversions at the reactor outlet were 20% for methane and 81% for oxygen. The paths to and among the C_3 components are not discussed, because the corresponding yields were too low. Also the following discussion concerns the chains which determine the selectivities of the oxidative coupling of methane beyond the primary initiation period.

		σ	$\vec{r}$	$\vec{r}$
Propagation/Branching				
$CH_4 + HO_2\cdot$	$\xrightarrow{5}$ $CH_3\cdot + H_2O_2$	1	0.31	14
$H_2O_2 + M$	$\xrightarrow{38}$ $2\ OH\cdot + M$	1	0.28	13
$CH_4 + OH\cdot$	$\xrightarrow{4}$ $CH_3\cdot + H_2O$	2	1.2	57
$C_2H_6 + CH_3\cdot$	$\xrightarrow{19}$ $C_2H_5\cdot + CH_4$	1	0.15	3.2
$O_2 + C_2H_5\cdot$	$\xrightarrow{22}$ $HO_2\cdot + C_2H_4$	1	0.061	3.3
$2\ CH_4 + O_2 + C_2H_6 \longrightarrow 2\ CH_3\cdot + C_2H_4 + 2\ H_2O$				
Termination				
$2\ CH_3\cdot + M$	$\xrightarrow{9}$ $C_2H_6 + M$		0.40	12

Figure 8. Typical branched chain towards methyl radicals, and the dominant termination.

Forward rates were calculated at the point in the reactor where $T = T_{max}$. Conditions: T_{max} = 1,078 K, δ = 4.0, left column: p_t = 100 kPa, right column: p_t = 400 kPa. The oxygen conversions at the point of calculation are the same and amount to 41% and the corresponding methane conversions are equal to 13% for p_t = 100 kPa and 12% for p_t = 400 kPa.

Branched chains

It has been established previously that the oxidative coupling of methane proceeds through a degenerate branched-chain mechanism (Chen et al., 1991), the most important branching step (Eq. 17) being the decomposition of hydrogen peroxide:

$$H_2O_2 + M \rightarrow 2\ OH\cdot + M \qquad (17)$$

This equation accounts almost totally for the production of radicals and thus hydrogen peroxide serves as the major radical source. Figure 8 shows an example of the branched chains which lead to methyl radicals. The hydrogen peroxide is formed for more than 9/10ths through a propagation step (Eq. 18):

$$CH_4 + HO_2\cdot \rightarrow CH_3\cdot + H_2O_2 \qquad (18)$$

The degeneration of the branched chain is caused by the dominant termination step (Eq. 19) corresponding to the coupling of one of the two most abundant radicals, $CH_3\cdot$, which accounts completely for the ethane formation:

$$2\ CH_3\cdot + M \rightarrow C_2H_6 + M \qquad (19)$$

The above description does not depend upon pressure nor conversion.

The total radical concentration in a reaction mixture remains constant at steady state, implying that the total radical production rate is equal to the total disappearance rate. Because step 38 (Eq. 17) and step 9 (Eq. 19) are the predominant radical producing and consuming steps, their rates should approximately be in balance at the steady state. The two rates are 0.28 and 0.40 $mol \cdot m^{-3} \cdot s^{-1}$ respectively at 100 kPa and 13 and 12 $mol \cdot m^{-3} \cdot s^{-1}$ respectively at 400 kPa. The rates of the two steps are not exactly equal, nor are the rates of the propagation steps after division by the appropriate stoichiometric numbers of the branched chain shown in Figure 8. This is due to the occurrence of several competing chains and of chain transfer steps between them.

Most abundant radicals

There are two most abundant radicals in the mixture (Chen and Marin, 1991), the methyl, $CH_3\cdot$, and the hydrogen peroxy radicals, $HO_2\cdot$. Their concentrations are in the order of magnitude of 10^{-4} $mol \cdot m^{-3}$, as calculated at the conditions given in Table 2 and several orders of magnitude higher than the other radicals.

Methyl Radicals. The high concentration of methyl radicals is caused by branched chains, viz. Figure 8. At all conditions, the direct formation of the methyl radical occurs via the following three steps in Table 2:

$$CH_4 + H\cdot \rightarrow CH_3\cdot + H_2 \quad (20)$$

$$CH_4 + OH\cdot \rightarrow CH_3\cdot + H_2O \quad (21)$$

$$CH_4 + HO_2\cdot \rightarrow CH_3\cdot + H_2O_2 \quad (22)$$

These account for more than 90% of the methyl-radical formation.

The disappearance of methyl radicals can be divided into three types: the recombination to ethane via step 9 in Table 2, the oxidation to carbon monoxide and the formation of methane by hydrogen atom abstraction. Each of the routes accounts for about one-third of the total methyl radical disappearance at atmospheric pressure (Chen et al., 1991). This picture does not change qualitatively at increased pressures.

The oxidation of methyl radicals proceeds via the sequence: $CH_3\cdot \rightarrow CH_3O\cdot \rightarrow CH_2O \rightarrow CHO\cdot \rightarrow CO$, independent of total pressure. Methyl radicals are first oxidized to methoxy radicals, $CH_3O\cdot$, which decompose into methanal, CH_2O. The instable methanal undergoes further decomposition readily to formyl radicals, $CHO\cdot$, which finally give rise to carbon monoxide:

$$CH_3\cdot + HO_2\cdot \rightarrow CH_3O\cdot + OH\cdot \quad (23)$$

$$CH_3O\cdot + M \rightarrow CH_2O + H\cdot + M \quad (24)$$

$$CH_2O + CH_3\cdot \rightarrow CHO\cdot + CH_4 \quad (25)$$

$$CHO\cdot + M \rightarrow CO + H\cdot + M \quad (26)$$

Hydrogen Peroxy Radicals. The other most abundant radical, $HO_2\cdot$, is neither produced in closed sequences analogous to the one shown in Figure 8, nor does it disappear in a termination step. It is exclusively formed directly from dioxygen, in particular through:

$$H\cdot + O_2 + M \rightarrow HO_2\cdot + M \quad (27)$$

This reaction was recently found to be one of the two most sensitive reactions for the $OH\cdot$ radical concentration in the reaction of a hydrogen-oxygen mixture (Baulch et al., 1990). The sensitivity analysis in the present study showed that it was one of the two most sensitive steps for $HO_2\cdot$, H_2O_2, and O_2 as well. At 100 kPa, step 36 in Table 2 accounts for half of the $HO_2\cdot$ formation, while at 400 kPa, this contribution increases to four-fifths. The rate of this step increases from 0.63 $mol \cdot m^{-3} \cdot s^{-1}$ at 100 kPa to 45 at 400 kPa. The disappearance of the $HO_2\cdot$ radical occurs dominantly via Eqs. 18 and 23.

Effect of total pressure on radical concentrations

As has been discussed previously, the $p_{1/2}$ value reported in Table 3 indicates that step 36 in Table 2 is of third-order at the pressures of interest. The disappearance of the $HO_2\cdot$, however, occurs via second-order reactions. This reaction order difference results in a concentration increase of a factor of about 10 for this radical, when the total pressure increases from 100 to 400 kPa. Applying the quasi-steady-state approximation to the $HO_2\cdot$ radical taking into account only steps 36 and 5 in Table 2 and solving the $HO_2\cdot$ concentration from the corresponding continuity equation indeed leads to a concentration dependence upon the total pressure which is close to quadratic. Because the other oxygen-containing reactive species, $OH\cdot$, H_2O_2, $CHO\cdot$, and $CH_3O\cdot$, are formed via $HO_2\cdot$ in second-order reactions and their disappearance occurs also via second-order reactions, it follows from the steady-state approximation that their concentrations are proportional to the $HO_2\cdot$ concentration and, hence, increase also by a factor of 10. As a result, the conversions and space-time yield increase exponentially with the total pressure, Figure 6.

The corresponding increase of $CH_3\cdot$ radicals amounts to a factor of 5. This can again be attributed to the different reaction orders of the radical formation and disappearance. The methyl-radical formation from methane, as well as the methyl-radical disappearance to ethane or CO, are of second order. However, the global orders for these reactions are higher than two and close to three, because radicals like $OH\cdot$, $HO_2\cdot$, $CHO\cdot$ and $CH_3O\cdot$ are involved. The reaction order for step 9 in Table 2 is between two and three and close to two, because this reaction is in the intermediate pressure fall-off region and quickly shifts towards second-order kinetic with increasing pressure because of its low $p_{1/2}$ values, Table 3. Therefore, the global order of the reaction of the methyl-radical production is higher than that of its disappearance, and hence, the pressure effect is slightly more than linear on the methyl-radical concentration. Application of the quasi-steady-state approximation to the $CH_3\cdot$ radical taking into account only steps 4 and 9 in Table 2 now leads to a dependence of its concentration upon the total pressure which is indeed slightly stronger than linear. The above considerations are also in line with the observed pressure dependence of the methane conversion rate and space-time yield of C_2 products.

Branched chains revisited

With the exponential increase of the oxygen-containing reactive species, the increases in reaction rates of the elementary

steps as shown in Figure 8 can easily be explained. Note that the concentration of the third body M increases almost exactly by a factor of 4, since it is determined essentially by the nonlimiting reactant methane. The ratio of the reaction rates at 400 and 100 kPa for the initiation, step 1 in Table 2, is 16, as expected. The corresponding increase in the rates of step 9 in Table 2, the recombination of two methyl radicals, amounts to 30. Since the methyl-radical concentration is increased by a factor of 5, a slightly larger increase than a factor of 25 is expected. An increase of the reaction rate to an even larger extent, that is, 40 is observed for the branching step 38 in Table 2, because the H_2O_2 concentration increases by a factor of 10 and that of the third body by a factor of 4.

The propagation steps in the branched chain for the methyl-radical production in Figure 8 show that the rates of the forward steps of 5, 38 and 4 in Table 2 have increased by a factor of approximately 40, when the total pressure is increased from 100 to 400 kPa. The corresponding factor for step 19 in Table 2 is 20. The factor 40 results from the fact that one of the reactants in these steps is $HO_2\cdot$, H_2O_2, or $OH\cdot$ whose concentrations increase by a factor of 10, and that the other reactant is methane, the third body M or dioxygen whose concentration increases by a factor of 4. The factor of 20 for the rate increase of step 19 can be explained similarly.

Chains to ethylene

Different concentration increases between the oxygen-containing and nonoxygen-containing radicals, as described previously, cause the shifts in the importance of different reaction paths between 100 and 400 kPa. Ethylene originates exclusively from ethane via ethyl radicals which are formed through hydrogen abstractions by mainly methyl radicals (Chen et al., 1991). Two types of chains lead from ethane to ethylene in this way, one pyrolytic and the other oxidative:

$$C_2H_5\cdot + M \rightleftharpoons C_2H_4 + H\cdot + M \qquad (28)$$

$$C_2H_5\cdot + O_2 \rightarrow C_2H_4 + HO_2\cdot \qquad (29)$$

At atmospheric pressure, the pyrolytic chain dominates and reaction 21 in Table 2 is in equilibrium (Chen et al., 1991). When the pressure is increased to 400 kPa, reaction 21 still stays close to equilibrium, as indicated by the affinity reported in Table 2. The contribution of both reactions towards the ethylene formation has become comparable, however. The ratios of the contributions of reactions 21 and 22 in Table 2 are respectively 4.0 and 1.8 at 100 and 400 kPa.

The former number agrees well with the conclusions from the previous study that at 100 kPa the pyrolytic chain contributes to the ethylene formation about three to four times as much as the oxidative chain. The contribution from the oxidative route has increased largely by raising the pressure due to the fact that step 21 in Table 2 is a unimolecular reaction while step 22 is bimolecular. Although the bimolecular nature of the latter reaction was recently questioned in the literature and pressure-dependent rate coefficients were calculated (Bozzelli and Dean, 1990), it is justified for the present modeling study to consider it as an elementary bimolecular process. At 100 kPa, step 21 is close to the low-pressure region, Table 2, and thus of a reaction order between first and second. With the increase of pressure, it shifts to first-order, whereas step 22 remains of second-order. Thus, the increase of pressure affects the oxidative step 22 more strongly than the pyrolytic step 21 in Table 2.

Table 4. Ratios of the Major Primary and Consecutive CO-Formation Rates to the Methyl-Radical Coupling Rate and Differential C_2 Selectivities at Conditions Corresponding to Figure 8

Pres. /100 kPa	X_{O2} = 41%			X_{O2} = 95%*		
	r_8/r_9	r_{30}/r_9	S_D/%	r_8/r_9	r_{30}/r_9	S_D/%
1	1.2	0.2	43	0.6	0.7	14
4	2.5	0.09	36	0.9	0.5	23

* For this case, the reactor temperatures downstream of the position where $T = T_{max}$ were kept at T_{max} until 95% conversion was reached

Chains to carbon monoxide

Two sources exist for the formation of carbon monoxide. The chains of oxidation of methyl radicals to CO are referred to as primary, whereas the consecutive chains include the oxidation of the C_2 components, either molecules or radicals, in which carbon-carbon bond fission accompanies the oxidation.

Primary Chains. In the primary chains, methyl radicals are oxidized via a series of intermediates and finally give rise to carbon monoxide, predominantly via steps 8, 10, 13 and 14 in Table 2, as discussed in the paragraph on methyl-radicals. Note that all four steps proceed at the same rates, Table 2. The oxidation step, 8, contributes for one-fourth to the total methyl-radical consumption at 100 kPa and the share increases to one-third at 400 kPa. In other words, the fraction of the methyl radicals which ends up as CO increases with the increase of pressure. This is also illustrated by Table 4, which shows the differential primary CO formation factors calculated at 100 and 440 kPa at two oxygen-conversion levels, 41% and 95%. The differential primary CO-formation factor is defined as the ratio of the rate of step 8 to that of step 9 in Table 2 at a certain position in the reactor. This factor compares the two steps which compete for methyl radicals: the higher the factor, the more competitive the oxidation. It can be seen that the primary factors are higher at 400 kPa than at 100 kPa. The above observations can be explained because chain carrier $HO_2\cdot$ is involved in step 8 in Table 2. Consequently, the integral C_2 selectivity decreases with increasing pressure, Figure 7. This decrease, however, is confined at low oxygen conversions, that is, to the left half of Figure 7. The decrease becomes smaller with increasing oxygen conversions and finally disappears, the right half of Figure 7. This can be attributed to the pressure effect on the consecutive reactions, which will be discussed next.

Consecutive Chains. In the consecutive routes towards CO the intermediates such as methanal, CH_2O, and formyl, $CHO\cdot$ are formed as a result of oxidative fission of the C-C bond in C_2 species:

$$C_2H_5\cdot + HO_2\cdot \rightarrow CH_3\cdot + CH_2O + OH\cdot \qquad (30)$$

$$C_2H_4 + OH\cdot \rightarrow CH_3\cdot + CH_2O \qquad (31)$$

$$C_2H_3\cdot + O_2 \rightarrow CH_2O + CHO\cdot \qquad (32)$$

Half of the fission occurs through reaction 30 in Table 2 (Eq. 32). Analogous reactions of ethane have been reported to be unimportant (Chen et al., 1991; Mackie, 1991). Ethyne oxidation to carbon monoxide has been established in the combustion literature, especially in the case of the oxidation of ethane (Warnatz, 1983, 1984). This involves intermediates such as $CH_2CO\cdot$, $CH_2\cdot$, and $CH\cdot$. Such a path has been considered during the development of the model. It turned out that the corresponding contributions towards the formation of carbon monoxide were negligible with respect to the other consecutive paths. Hence, this path was not included in the final model.

The oxidation of C_2 products to CO plays a significant role in limiting the C_2 selectivity: more than half of the ethane which reacts further leads finally to CO at 400 kPa. This conclusion results from the following analysis. About 99% of ethane which disappears is converted into ethyl radicals. Hence, the fraction of the ethyl radicals which ends up in CO can be considered as the corresponding fraction for ethane. Less than one-tenth of the ethyl radical disappears to form CO precursors, reaction 20 in Table 2, nine-tenths ends up as ethylene, and a small fraction leads to C_3 products. Similarly, ethylene disappears along three paths, the major one being the reaction to vinyl radicals and C_3 components, which accounts for two-thirds of the total ethylene disappearance. One-fifth disappears via reaction 27 in Table 2 to CO precursors. Taking into account that nine-tenths of the ethyl radicals goes to ethylene, a one-fifth disappearance of ethylene to CO is approximately equivalent to *one-fifth* of the ethyl-radical disappearance. Similarly, half of the vinyl radical which disappears leads to CO precursors via reaction 30 corresponding to approximately *three-tenths* of the ethyl-radical disappearance. Summarizing, roughly half of the ethyl radical and thus also of the ethane which disappears is converted into CO. In spite of this, however, the contribution to the CO formation from C_2 is still much less than that from the methyl radical. This is due to the fact that the total amount of C_2 products never exceeds 10 mol %, while the methane concentration is about 50% even at a methane conversion of 30%.

Table 4 shows also the differential consecutive CO formation factors defined as the ratio of the reaction rate of step 30 in Table 2, the major consecutive oxidation of the C_2 products, to that of reaction 9 in Table 2, the production of C_2. The factors indicate clearly that high pressures do not favor the consecutive oxidations. This is due to the weaker pressure dependence of step 30 when compared to step 9. As a consequence, less C_2 disappears to CO at 400 kPa than at 100 kPa and, hence, the differential C_2 selectivity decreases also less strongly at 400 kPa, as can be seen from Table 4. The differential C_2 selectivity on the carbon-atom basis is, by definition, the ratio of the production rate of the C_2 components to the consumption rate of methane and can be easily calculated:

$$S_D = \frac{r_{f,C_2} - r_{d,C_2}}{r_{d,C_1}} = \frac{2r_9 - 2(r_{20} + r_{27} + r_{30})}{2r_9 + (r_6 + r_7 + r_8)} \tag{33}$$

The results shown in Figure 7 can now be rationalized as follows. At low conversions, the primary chains dominate the CO formation and determine the differential and, hence, also the integral C_2 selectivity. With the increase of conversions, however, consecutive chains become more important gradually. Because increasing pressure then becomes beneficial to the differential C_2 selectivity, the integral C_2 selectivity at 400 kPa catches up with that at 100 kPa. The balance between the primary and consecutive chains towards CO, therefore, determines the integral C_2 selectivity over the complete conversion range.

Conclusions

At constant temperature and residence time, the conversions of methane and oxygen increase with increasing pressure. Space-time yields of C_2 products increase sufficiently to reach a level comparable to that required for industrial operations. At low conversions, the integral selectivity to ethylene decreases by 4 to 8% with a pressure increase from 100 to 400 kPa. This decrease is accompanied with an increase of the integral selectivity to CO. With the increase of the conversion, this decrease becomes smaller and disappears at oxygen conversions of 80%.

A kinetic model consisting of 38 elementary radical reactions allows an adequate calculation of the feed conversions and product selectivities over the complete range of conditions investigated. The pressure fall-off behavior of unimolecular reactions was found to be essential in describing the pressure effect observed experimentally.

The general features of the reaction mechanism do not depend on the total pressure. The methyl, $CH_3\cdot$, and the hydrogen peroxy, $HO_2\cdot$, are the most abundant radicals. The reaction proceeds through branched chains, the decomposition of hydrogen peroxide being the branching step. The branched chain is degenerated via the coupling of two methyl radicals, resulting in the desired product ethane.

The total pressure increase results in an exponential increase of concentrations of oxygen-containing chain carriers which causes the strong increase of the conversion rates and space-time yields. The dependence of the methyl-radical concentration on the total pressure is only slightly stronger than linear. The different concentration increases between the oxygen-containing chain carriers and the methyl radical cause the shifts in the importance of different reaction paths.

The dehydrogenation of ethane to ethylene proceeds via pyrolytic and oxidative chains. The latter are favored at higher pressures because of their higher reaction order. The balance between the primary and consecutive chains towards CO determines the integral C_2 selectivity. The fraction of methyl radicals which is oxidized to CO increases at higher pressures. This can be attributed to the fact that the increase of the methyl-radical concentration is smaller than the increase of the concentrations of the oxygen-containing chain carriers and results in a decrease of the integral C_2 selectivity at low oxygen conversions. At sufficiently high oxygen conversions, the consecutive chains towards CO become dominant. Increasing pressure is now beneficial to the differential C_2 selectivity because of the less pronounced pressure dependence of these chains when compared to that of the coupling. Therefore, the integral C_2 selectivity at high oxygen conversions becomes comparable to the selectivity at atmospheric pressure. The major contribution to the integral CO selectivity comes from the oxidation of methyl radicals.

Acknowledgment

The financial support by the Commission of the European Com-

munities in the framework of the Joule program, subprogram Energy from Fossil Sources, Hydrocarbons, No. JOUF-0044-C, is gratefully acknowledged.

Notation

A = preexponential factor, 1st-, 2nd- and 3rd-order reaction, s^{-1}, $m^3 \cdot mol^{-1} \cdot s^{-1}$, $m^6 \cdot mol^2 \cdot s^{-1}$, respectively
A = affinity of a reaction, $kJ \cdot mol^{-1}$
A_i = peak area from GC analysis
C = concentration, $mol \cdot m^3$
d_i = response factor of species i in GC analysis
E_a = activation energy, $kJ \cdot mol^{-1}$
F_i = molar flow rate of component i, $mol \cdot s^{-1}$
k_u = constant for rate coefficient of unimolecular reactions
K = equilibrium constant
l = total length of reactor, m
M = third body
$n_{j,i}$ = number of atoms of element j in species i
p = pressure, Pa
r_i = rate of reaction i, $mol \cdot m^{-3} \cdot s^{-1}$
r_i = rate of the forward step of reaction i, $mol \cdot m^{-3} \cdot s^{-1}$
r_i = rate of the backward step of reaction i, $mol \cdot m^{-3} \cdot s^{-1}$
R = gas constant, 8.314×10^{-3}, $kJ \cdot mol^{-1} \cdot K^{-1}$
S_D = differential selectivity to C_2 products
S_{ij} = selectivity to i with respect to feed j
T = temperature, K
V = reactor volume, m^3
w = weighting factor
X = conversion of feed component
z = length coordinate along the reactor, m

Greek letters

δ = methane to oxygen ratio at the inlet of reactor, $mol \cdot mol^{-1}$
σ = stoichiometric number
τ = residence time, s
Ω = cross-sectional area of reactor, m^2

Subscripts

0 = reactor inlet; low-pressure limit
1/2 = center of the fall-off curve where $k_u/k_\infty = 1/2$
b = bimolecular
d = disappearance
D = differential
f = formation
I = initiation
∞ = high-pressure limit
M = third body
max = maximum
t = total
T = termination
u = unimolecular

Literature Cited

Asami, K., K. Omata, K. Fujimoto, and H. Tominaga, "Vapor-Phase Oxidative Coupling of Methane under Pressure," *Energy & Fuels*, **2**, 574 (1988).

Baerns, M., and J. R. H. Ross, "Catalytic Chemistry of Methane Conversion," *Perspective in Catalysis*, J. M. Thomas and K. I. Zamaraev, eds., IUPAC monograph, Blackwell Scientific Publications, Oxford (1992).

Baulch, D. L., J. F. Griffiths, B. Johnson, and R. Richter, "Hydroxyl Radical Concentrations and Reactant Temperature Profiles during Oscillatory Ignition of Hydrogen: Experimental Measurements by Laser Resonance Absorption Spectroscopy and Comparisons with Numerical Calculations," *Proc. R. Soc. Lond. A*, **151**, 430 (1990).

Benson, S. W., *Thermochemical Kinetics*, 2nd ed., Wiley, New York (1976).

Bozzelli, J. W., and A. M. Dean, "Chemical Activation of the Reaction of C_2H_5 with O_2," *J. Phys. Chem.*, **94**, 3313 (1990).

Brophy, J. H., and R. P. Manning, "Conversion of Hydrocarbons," EP 0178855 A2 (1985).

Chen, Q., J. H. B. J. Hoebink, and G. B. Marin, "Kinetics of the Oxidative Coupling of Methane at Atmospheric Pressure in the Absence of Catalyst," *Ind. Eng. Chem. Res.*, **30**, 2088 (1991).

Chen, Q., and G. B. Marin, "Production of Ethene from Natural Gas. The Oxidative Coupling of Methane in the Absence of Catalyst under Elevated Pressure," *Proc. of Interpec*, Beijing, China (1991).

Chen, Q., J. H. B. J. Hoebink, and G. B. Marin, "Process Research and Development for the Partial Oxidation of Methane to C_2 Hydrocarbons," *Proc. of EuroGas*, Trondheim, Norway (1992).

Choudhary, V. R., S. T. Chaudhari, and A. M. Rajput, "Oxidative Pyrolysis of Methane to Higher Hydrocarbons: Effects of Water in Feed," *AIChE J.*, **37**, 915 (1991).

Cleland, F. A., and R. H. Wilhelm, "Diffusion and Reaction in Viscous-flow Tubular Reactor," *AIChE J.*, **2**, 489 (1956).

Dente, M., E. Ranzi, and A. G. Goossens, "Detailed Prediction of Olefin Yields from Hydrocarbon Pyrolysis through a Fundamental Simulation Model (SPYRO)," *Computer and Chem. Eng.*, **3**, 61 (1979).

Ekstrom, A., R. Regtop, and S. Bhargava, "Effect of Pressure on the Oxidative Coupling Reaction of Methane," *Appl. Catal.*, **62**, 253 (1990).

Foulds, G. A., B. F. Gray, J. F. Griffiths, and G. S. Walker, "Theoretical Modeling of the Gas Phase Partial Oxidation of Methane," Preprint, paper presented at Amer. Chem. Soc. meeting, San Francisco (Apr. 5-10, 1992).

Gardiner, W. C., and J. Troe, "Rate Coefficients of Thermal Dissociation, Isomerization, and Recombination Reactions," *Combustion Chemistry*, Chap. 4, W. C. Gardiner, ed., Springer Verlag, New York (1984).

Geerts, J. W. M. H., Q. Chen, J. M. N. Van Kasteren, and K. Van Der Wiele, "Thermodynamics and Kinetic Modeling of the Homogeneous Gas Phase Reactions of the Oxidative Coupling of Methane," *Catal. Today*, **6**, 519 (1990).

Hargreaves, J. S. J., G. J. Hutchings, and R. W. Joyner, "Control of Product Selectivity in the Partial Oxidation of Methane," *Nature*, **348**, 428 (1990).

Howard, M. J., "The Homogeneous Partial Oxidation of Methane-Containing Paraffinic Hydrocarbon," EP 0302665 A1 (1989).

Hutchings, G. J., M. S. Scurrell, and J. R. Woodhouse, "The Role of Gas Phase Reaction in the Selective Oxidation of Methane," *J. Chem. Soc., Chem. Commun.*, 253 (1989).

Labinger, J. A., and K. C. Ott, "Mechanistic Studies on the Oxidative Coupling of Methane," *J. Phys. Chem.*, **91**, 2682 (1987).

Lane, G. S., and E. E. Wolf, "Methane Utilization by Oxidative Coupling I. A Study of Reactions in the Gas Phase during the Cofeeding of Methane and Oxygen," *J. Catal.*, **113**, 144 (1988).

Lunsford, J. H., "The Catalytic Conversion of Methane to Higher Hydrocarbons," *Catal. Today*, **6**, 235 (1990).

Mackie, J. C., "Partial Oxidation of Methane: The Role of the Gas Phase Reactions," *Catal. Rev.-Sci. and Eng.*, **33**, 169 (1991).

McCarty, J. G., "Mechanism of Cooxidative Methane Dimerization Catalysis: Kinetic and Thermodynamic Aspects," *Methane Conversion by Oxidative Processes. Fundamental and Engineering Aspects*, E. E. Wolf, ed., Van Nostrand Reinhold, New York, p. 321 (1992).

Onsager, O. T., R. Lodeng, P. Soraker, A. Anundskaas, and B. Helleborg, "The Homogeneous Gas Phase Oxidation of Methane and the Retarding Effect of Basic/Inert Surfaces," *Catal. Today*, **4**, 355 (1989).

Plehiers, P. M., and G. F. Froment, "Reversed Split Coil Improves Ethylene Yields," *Oil & Gas J.*, 41 (Aug. 17, 1987).

Robinson, P. J., and K. A. Holbrook, *Unimolecular Reactions*, Wiley-Interscience, London (1972).

Semenov, N., *Some Problems in Chemical Kinetics and Reactivity*, Vol. II, translated from Russian by M. Boudart, Princeton University Press, Princeton, NJ (1958).

Tjatjopoulos, G. J., and I. A. Vasalos, "Reaction-path Analysis of a Homogeneous Methane Oxidative Mechanism," *Appl. Catal.*, **88**, 213 (1992).

Tsang, W., "Chemical Kinetic Database for Combustion Chemistry: 3. Propane," *J. Phys. Chem. Ref. Data*, **17**, 887 (1988).

Tsang, W., and R. F. Hampson, "Chemical Kinetic Data Base for Combustion Chemistry: Part 1. Methane and Related Compounds," *J. Phys. Chem. Ref. Data*, **15**, 1087 (1986).

Tulenin, Yu. P., A. A. Kadushin, V. A. Seleznev, A. F. Shestakov,

and V. N. Korchak, "Effect of Pressure on the Process of Methane Oxidative Dimerization: I. The Mechanism of Heterogeneous Inhibition of the Gas Phase Reactions," *Catal. Today*, **13**, 329 (1992a).
Tulenin, Yu. P., A. A. Kadushin, V. A. Seleznev, A. F. Shestakov, and V. A. Menshikov, "Effect of Pressure on the Process of Methane Oxidative Dimerization: II. The Catalyzed Reaction in Conditions of Suppression of the Gas Phase Reactions," *Catal. Today*, **13**, 523 (1992b).
Walsh, D. E., D. J. Martenak, S. Han, and R. E. Palermo, "Direct Oxidative Methane Conversion at Elevated Pressure and Moderate Temperatures," *Ind. Eng. Chem. Res.*, **31**, 1259 (1992).
Warnatz, J., "Hydrocarbon Oxidation at High Temperatures," *Ber. Bunsenges. Phys. Chem.*, **87**, 1008 (1983).
Warnatz, J., "Rate Coefficients in the C/H/O System," *Combustion Chemistry*, Chap. 5, W. C. Gardiner, ed., Springer Verlag, New York (1984).
Weisz, P. B., "Windows on Reality," *CHEMTECH*, 424 (July 1982).
Yarlagadda, P. S., L. A. Morton, N. R. Hunter, and H. D. Gesser, "Direct Conversion of Methane to Methanol in a Flow Reactor," *Ind. Eng. Chem. Res.*, **27**, 252 (1988).
Zanthoff, H., and M. Baerns, "Oxidative Coupling of Methane in the Gas Phase, Kinetic Simulation and Experimental Verification," *Ind. Eng. Chem. Res.*, **29**, 2 (1990).

Manuscript received Feb. 22, 1993, and revision received July 9, 1993.